Inorganica Chimica Acta 465 (2017) 50–60

Contents lists available at ScienceDirect

Inorganica Chimica Acta

journal homepage: www.elsevier.com/locate/ica

Research paper

A detailed study on the interaction of a novel water-soluble glycine bridged zinc(II) Schiff base coordination polymer with BSA: Synthesis, crystal structure, molecular docking and cytotoxicity effect against A549, Jurkat and Raji cell lines

Zahra Asadi [a,*], Maryam Golchin [a], Vaclav Eigner [b], Michal Dusek [b], Zahra Amirghofran [c]

[a] Department of Chemistry, College of Sciences, Shiraz University, Shiraz 71454, Iran
[b] Institute of Physics ASCR, v.v.i, Na Slovance 2, 182 21 Prague, Czech Republic
[c] Department of Immunology and Medicinal and Natural Products Chemistry Research Center, Shiraz University of Medical Sciences, Shiraz 71454, Iran

ARTICLE INFO

Article history:
Received 24 March 2017
Received in revised form 28 May 2017
Accepted 29 May 2017
Available online 30 May 2017

Keywords:
Water-soluble
Coordination polymer
BSA
Docking study
Anticancer activity

ABSTRACT

A novel water-soluble glycine bridged zinc(II) Schiff base coordination polymer was synthesized by the condensation of 2,6-diformyl-4-methylphenol, glycine, and zinc(II) chloride. The complex was characterized by ^{1}HNMR, FT-IR, elemental analyses and X-ray crystallography. The polymeric complex was built up of two glycine-bridged Zn/L moieties, where L denotes the Schiff base containing 2,6-diformyl-4-methylphenol and glycine in 1:1 M ratio. The carboxylic group of L was coordinated to the Zn atoms of the neighboring moieties; thus each Zn center was five-coordinated. The interaction between polymeric Zn(II) complex and bovine serum albumin (BSA) was studied by UV–Vis, fluorescence, and synchronous fluorescence spectroscopic techniques. By considering the sign and values of the thermodynamic parameters (ΔH and ΔS), it is clear that the binding between BSA and complex was exothermic and entropy-driven and electrostatic interactions between the complex and BSA was supposed. Site-selective binding studies revealed that the complex were mainly located in the region of site II (subdomain IIIA) in BSA. From the synchronous fluorescence spectroscopic studies, it is concluded that complex could bind to tyrosine and tryptophan residues simultaneously. The K_b values indicated a high binding affinity of the complex to BSA. In vitro anticancer activity of the polymeric Zn(II) complex was evaluated against A549, Jurkat, and Raji cell lines by MTT assay. The complex was remarkably active against the cell lines and can be a good candidate for an anticancer therapy. Theoretical docking studies were performed to further investigate the BSA binding interactions.

1. Introduction

Studies of coordination polymers (CPs) has been started since 1989 by Robson and Hoskins [1,2]. Coordination polymers (CPs) arising from the interaction between metal ions and multidentate ligands exhibit structural diversities due to various possibilities for metal ions and ligands. The application of CPs in the different fields such as gas storage/separation [3–11], sensors [12–14], catalysis [15–22], photonics [23,24] and magnetism [25–29] is studied [30]. In the preparation of coordination polymers, some special ligands such as phenyldicarboxylates are widely employed because of their extraordinary varieties in the binding of complexes [31]. Also the selection of the metals is very important in designing CPs. Divalent metal ions of first-transition-row such as Co(II), Ni(II), Cu(II) and Zn(II) are good candidates as metal sources due to their low cost and safety in industrial and biological applications [32]. It is worthy to note that first row transition metals are essential for many important chemical processes in biological systems. Zn(II) complexes have been widely reported as radioprotective agents [33], tumor photosensitizers [34], antidiabetic insulin-mimetics [35,36], and antibacterial or antimicrobial [37–39] agents. Amino acid derived Schiff base ligands support the binding of metal ions rather frequently.

One of the most important challenges in designing metal complexes for drug delivery is the metal effect on the cancer treatment. Recently some studies comparing mono- and binuclear metal complexes as anticancer drugs have been reported [40–45]. The diversity in the coordination number, geometries, redox states, thermodynamic-kinetic characteristics and intrinsic properties of

* Corresponding author.
E-mail address: zasadi@shirazu.ac.ir (Z. Asadi).

http://dx.doi.org/10.1016/j.ica.2017.05.066
0020-1693/

metal ions and ligands are important in cancer therapy. It is proven that multinuclearity increases the efficiency and selectivity of the anticancer drugs due to the potential cooperation between the metal centers [41,46–52]. Recently, CPs and metal organic frameworks (MOFs) with multi-metal centers have attracted intense attention in cancer therapy [53] and multi-carrier of drugs [54]. Many drugs are bound to albumin and transported in the blood. Thus formation of complexes between drugs and proteins are important from the point of view of transportation and mechanism of drug-protein interaction and search of new drug molecules [53,55–64]. In this study, bovine serum albumin (BSA) as the protein model is used. Its medical importance as a circulating protein, its abundance, low cost, availability, ease of purification, ability to produce an intrinsic fluorescence emission, and structural similarity with human serum albumin (HSA) are the reasons for this selection [65,66].

In this paper we report synthesis and characterization of a water soluble glycine bridged zinc(II) Schiff base coordination polymer. In designing the complex, we expected a bimetallic Schiff base complex but to our surprise a coordination polymer was synthesized. By considering the unique structure and application of CPs, the pharmacological properties of the complex were investigated in detail.

2. Experimental section

2.1. Material and measurements

Bovine serum albumin (BSA), phenylbutazone, ibuprofen, p-cresol, hexamethylenetetramine, paraformaldehyde, 2-aminoethanol, glycine, zinc (II) chloride, sodium nitrate, methanol, ethanol, sulfuric acid, acetic acid, toluene, diethyl ether, *n*-hexane, chloroform, dimethylsulfoxide (DMSO), NaCl and Tris for buffer solution, DMSO-d_6, $CDCl_3$ and D_2O for NMR spectroscopy, potassium bromide (KBr) for IR spectroscopy were obtained from Merck, Fluka, Sigma and Aldrich.

The NMR spectra were recorded on Bruker Avance DPX 250 MHz spectrometer. UV–Vis. measurements were carried out on Perkin-Elmer (LAMBDA 2) UV–Vis. spectrophotometer equipped with a LAUDA-ecoline-RE 104 thermostat at different temperatures. FT-IR spectra were recorded on Shimadzu FT-IR 8300 infrared spectrophotometer. Elemental analysis (C.H.N.) was carried out on Thermo Finnigan-Flash 1200. Melting points of compounds were measured with BUCHI 535. The X-ray diffraction measurements were made at 95 K on a SuperNova diffractometer of Rigaku Oxford Diffraction using the mirror-collimated CuKα radiation from a micro-focus sealed X-ray tube and CCD detector Atlas S2. All experiments were carried out in triple distilled water at pH 7.4, 1 mM Tris buffer and 5 mM NaCl. Fluorescence and synchronous fluorescence measurement were carried out on a Perkin Elmer (LS 45) spectrofluorimeter.

2.2. Synthesis of 2,6-diformyl-4-methylphenol [67]

To a solution of p-cresol (10.8 g, 0.1 mol) in acetic acid (50 cm^3) were added hexamethylenetetramine (28.2 g, 0.2 mol) and paraformaldehyde (30 g, 1.0 mol). The system was stirred until a light brown viscous solution was formed and then heated (70–90 °C) for 2 h. The solution was cooled to room temperature and conc. H_2SO_4 (10 cm^3) added carefully. The resulting solution was refluxed again for 0.5 h and then on treatment with distilled water (400 cm^3) resulted in the formation of a light yellow precipitate, which was stored at 4 °C overnight. The yellow product was isolated by filtration and washed with a small amount of cold CH_3OH. A purer product was obtained after recrystallization from toluene.

Yield: 5.7 g (35%); color: yellow; m.p: 130–134 °C (lit., 133.5 °C); ^{1}H NMR [250 MHz, DMSO-d_6, δ (ppm)]: 11.38 (s, 1H, OH), 10.19 (s, 2H, HC═O), 7.82 (s, 2H, Ar-H), 2.31 (s, 3H, CH_3); ^{1}HNMR ($CDCl_3$, ppm): 11.39 (s, 1H, OH), 10.15 (s, 2H, HC═O), 7.70 (s, 2H, Ar-H), 2.32 (s, 3H, CH_3); FT-IR (KBr, cm^{-1}): 2869 ($\upsilon_{C\text{-}H}$), 1674 ($\upsilon_{C=O}$), 1211 ($\upsilon_{C\text{-}O}$); Elemental Analysis, Found (Calc.)%: $C_9H_8O_3$ (MW = 164.05 g.mol^{-1}) C: 66.02 (65.85); H: 4.78 (4.91); N: 0 (0).

2.3. Synthesis of polymeric complex

To a solution of 2,6-diformyl-4-methylphenol (0.16 g, 1 mmol) in 20 mL ethanol was added a solution of glycine (0.15 g, 2 mmol) in 10 mL water. The reaction mixture was refluxed. After 3 h zinc (II) chloride (0.27 g, 2 mmol) was added to the solution. A yellow solid precipitate was collected by filtration after solvent evaporation and washed with cold ethanol and diethyl ether. Yellow crystals suitable for X-ray crystallography were obtained by recrystallization in water.

Yield: 0.53 g (48%); color: yellow; m.p: 280 °C; FT-IR (KBr, cm^{-1}): 3448 (υ_{OH}), 1658 ($\upsilon_{C=O}$), 1542 ($\upsilon_{C=N}$); Elemental Analysis, Found (Calc.)%: $C_{26}H_{24}N_4O_{10}Zn_2{\cdot}4H_2O$ (MW = 755.33 g.mol^{-1}) C: 41.85 (41.34); H: 4.36 (4.27); N: 7.59 (7.42).

2.4. Protein-binding study

2.4.1. Absorption spectra

Electronic absorption spectra were recorded on a Perkin-Elmer (Lambda 2) UV–Vis spectrophotometer, equipped with thermostat. The wavelength range was from 250 to 500 nm at 293, 298, 303 and 308 K. Absorption spectral titrations were carried out in Tris-HCl buffer (pH = 7.4) for the free proteins (bovine serum albumin) (2×10^{-5} M) in the absence and presence of the complex (8×10^{-4} M) in the same buffer. The mixture in the cuvette was shacked homogeneously before each scan.

2.4.2. Fluorescence spectra

Intrinsic fluorescence of proteins makes the fluorescence spectroscopy as a reliable technique in the study of drug-protein interaction. The fluorescence emission spectra of BSA were scanned in the range 300–500 nm using an excitation wavelength of 280 nm. In a fluorescence measurement, 2.5 mL of serum albumin solutions (bovine serum albumin) (pH 7.4) with the concentration of 7.2×10^{-8} M in 1 mM Tris buffer and 5 mM NaCl was added accurately to the quartz cell of 1 cm optical path and titrated by successive additions of complex (5×10^{-5} M) (0–55 μL) in the same buffer in the time intervals equal to 3 min. So the change in fluorescence emission intensity was measured within 3 min after each addition of the complex to bovine serum albumin.

2.4.3. Site marker competitive experiments

Binding location studies between the complex and bovine serum albumin (BSA) in the presence of phenylbutazone (site marker of site I) and ibuprofen (site marker of site II) were measured using the fluorescence titration methods. For this purpose, a mixture of 2.5 mL BSA (7.2×10^{-8} M) and 10 μL phenylbutazone (1.8×10^{-5} M in 50/50 V/V% water/acetone) was kept for 1 h and titrated by complex solution. Similar solutions containing 10 μL ibuprofen (1.8×10^{-5} M in 50/50 V/V% water/acetone) and 2.5 mL BSA (7.2×10^{-8} M) were prepared and titrated with complex (5×10^{-5} M) (0–45 μL). Titration was followed by fluorescence spectroscopy using excitation wavelength of 280 nm.

2.4.4. Synchronous fluorescence spectra measurements

In the synchronous fluorescence spectra, the excitation and emission monochromator with a fixed wavelength differences (Δλ) between them was scanned simultaneously. Synchronous flu-

orescence spectroscopy is a useful technique to explore the structural changes of BSA by addition of the complex (5×10^{-5} M) (0–40 μL). The synchronous fluorescence spectra at the wavelength interval $\Delta\lambda = 15$ nm is due to the tyrosine residues and at the wavelength interval $\Delta\lambda = 60$ nm is due to the tryptophan residue of BSA [68].

2.4.5. The cytotoxicity assay

The growth inhibitory effects of the complex against three cell lines including Jurkat human T cell leukemia, Raji Burkitt's lymphoma and A549 lung carcinoma were examined by 3-(4,5-dimethylthiazol-2-yl)-2,5-diphenyltetrazolium bromide (MTT) assay as previously described [69]. The cell lines were cultured in RPMI 1640 medium (Sigma, St. Louis, MO) supplemented with 10% fetal calf serum (Gibco, Berlin, Germany). Cells were maintained at 37 °C with 5% CO_2 and 95% humidity. The cells were fed until confluent and expanded by trypsinization (for A549), then sub-cultured at lower numbers in new culture flasks. A predetermined number of cells (15×10^3 for Jurkat and Raji cells and 7.5×10^3 for A549 cells) were seeded in the wells of a 96-well plate with varying concentrations of the complex (0.1–100 μg/mL) and incubated at 37 °C with 5% CO_2 for 48 h. Cells treated only with dimethyl sulfoxide (solvent) at a concentration equal to the test wells was used as negative control and those treated only with *cisplatin* as positive control. 10 μL MTT solutions (5 mg mL^{-1} in RPMI medium) were added to each well and incubation was continued for 4 h. At the end, the produced insoluble formazan was dissolved by adding DMSO and shaking for 10 min. Then, the optical density (OD) was read at 570 nm with a reference wavelength of 630 nm in a microplate reader (Bio-Tek's ELx808, VT). To calculating the percentage of growth inhibition, the equation: [1 − (test OD/negative control OD)] × 100 was used. From the graph of inhibition percentage against different compounds concentrations the 50% cell inhibition (IC50) value was calculated.

2.4.6. Molecular docking

The crystal structure of BSA (PDB ID 3V03) was taken from the Brookhaven Protein Data Bank (http://www.pdb.org). 3V03 crystal structure was preferred for docking process because of no missing atoms, no crystallized ligand and reasonably good resolution. Docking calculations considering all flexible ligands were performed using the MVD program package. In order to allow the ligands to rotate freely even in their most fully extended conformations, the bonding site was chosen at (x = 37.81, y = 19.87, z = 58.18) with radius 13 Å. The docked conformation of the complexes with BSA was generated by the molecular docking program Molegro Virtual Docker (MVD) [70].

3. Results and discussion

3.1. Synthesis and characterization of the compounds

The synthetic route to the compounds is shown in Scheme 1. The synthesized compounds were identified by X-ray crystallography, FT-IR, ^{1}HNMR, electronic spectra and elemental analyses. The polymeric complex is stable in atmosphere for extended periods and soluble in water, DMSO and ethanol. It is insoluble in non-polar solvents.

The ^{1}H NMR spectrum of 2,6-diformyl-4-methylphenol was carried out in DMSO-d_6 and $CDCl_3$ (Fig. S1). ^{1}H NMR spectrum in DMSO-d_6 revealed a singlet signal at 11.38 ppm which was assigned to OH proton. A singlet signal of the aldehydic protons at 10.19 ppm and a singlet signal of the aromatic protons at 7.82 ppm were observed. Methyl protons were observed as a singlet signal at 2.31 ppm.^{1}H NMR spectrum of the polymeric complex was run in D_2O (Fig. S2). Two singlet signals at 8.20 and 8.26 ppm were assigned to HC═N protons, confirmed unequivalent chemical environment. Aromatic protons were displayed at 7.24–7.34 ppm. A signal for CH_3 protons at 3.39 ppm and signals for CH_2 protons at 2.10–2.18 ppm were observed. In the FT-IR spectrum of 2,6-diformyl-4-methylphenol a strong intensity band at 1674 cm^{-1} was assigned to the C═O group (Fig. S3). By comparing the FT-IR spectrum of the precursor aldehyde and the polymeric complex (Fig. S4), it was revealed that (C-O) stretching vibration shifts toward lower values as a result of coordination of oxygens to the metal ion [71]. (C═N) stretching vibration which was observed at 1685 cm^{-1} indicated the formation of imine bonds. Medium-weak bands at 2923 cm^{-1} for polymeric complex were related to (C—H) modes of vibrations [72]. The ring skeletal vibrations (C═C) were consistent in the region of 1440–1465 in the polymeric complex [73]. The electronic absorption spectrum of the CP (Tris-HCl buffer, 5×10^{-5} M), displayed two intense absorption bands at 216 and 243 nm which were assigned to phenyl and imine ($\pi \rightarrow \pi^*$) transitions, respectively. A wide weaker absorption band at 415 nm was related to imine ($n \rightarrow \pi^*$) transition (Fig. S5). The thermal decomposition of the complex was studied to evaluate its thermal stability. During the thermal analysis, heating rates were set to 20 °Cmin^{-1} under helium atmosphere, and the weight loss was measured from the ambient temperature up to 1000 °C. Two endothermic effects were revealed at 133.8 and 180.8 °C which confirmed that the complex was stable before 133.8 °C. It means that during the biological studies thermal decomposition was not been occurred (Fig. S6).

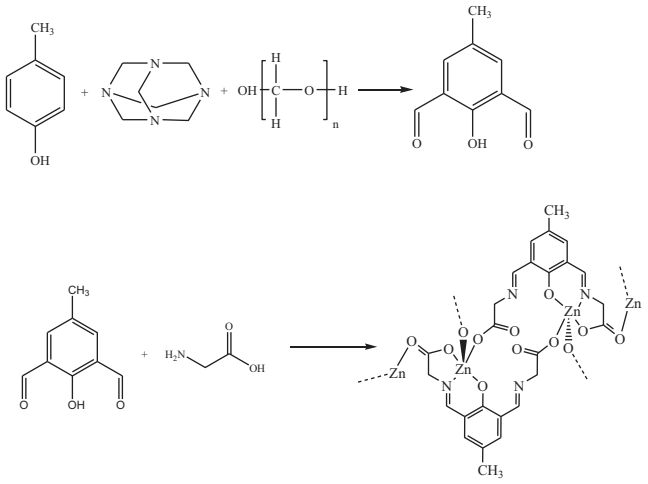

Scheme 1. The synthetic route to the compounds.

3.2. X-ray structure analysis

Yellow crystals suitable for X-ray crystallography were obtained by recrystallization in water. Structure was solved with Superflip [74] and refined with Jana2006 [75]. X-ray crystallography determination revealed that polymeric complex crystalized in the monoclinic space group P1 21/c1 with two formula units in the unit cell. The asymmetric units of complex comprise two Zn/L units and two bridging glycine molecules. The ORTEP view of the polymeric complex is shown in Figs. 1, 2. Crystallographic data and refinement parameters of the polymeric complex are listed in Tables 1, 2. The coordination environment about each zinc(II) center was a distorted square pyramidal with the phenolic oxygen, iminic nitrogen and oxygen atom of Schiff base and oxygen atom of the bridged glycine. These four atoms made a slightly distorted square coordination around Zn(II), and a carbonyl group of

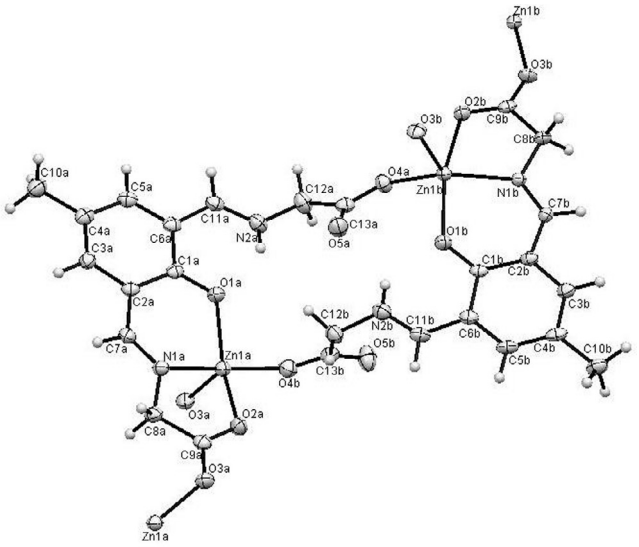

Fig. 1. An ORTEP view of the zinc(II) polymeric complex with the atom numbering scheme. One repeated unit of the polymeric complex is shown and four uncoordinated water molecules are omitted for clarity. Two similar but not symmetry-equivalent parts of the complex are distinguished by "a" and "b" suffixes.

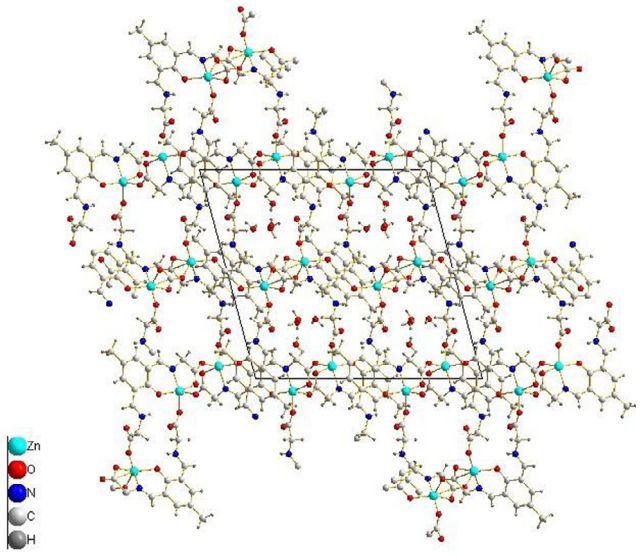

Fig. 2. Crystal structure of the polymeric complex.

the neighboring moiety was coordinated in the apical position, thus each Zn center is five coordinated. The coordination bond angles were 95.6(1)° (O4a-Zn1b-O1b), 87.9(1)° (O1b-Zn1b-N1b), 78.4(1)° (O2b-Zn1b-N1b), 85.7(1)° (O2b-Zn1b-O4a), respectively. The apical bond angles were 99.9(1)° (O4a-Zn1b-O3b), 117.5(1)° (N1b-Zn1b-O3b), 95.9(1)° (O2b-Zn1b-O3b), 104.0(1)° (O1b-Zn1b-O3b), respectively. These bond angles revealed that Zn atom was located out of the square plane. The bond distances around zinc center were 2.039(4), 2.027(3), 2.069(4), 1.959(4), and 2.020(3) for Zn1a-N1a, Zn1a-O1a, Zn1a-O2a, Zn1a-O4b, Zn1a-O3b (polymeric type), respectively.

3.3. Fluorescence quenching studies

Interaction of drugs with plasma proteins, particularly with serum albumin (the most abundant protein in plasma) is important especially in drug delivery and drug design studies. Bovine serum albumin is very useful in the protein studies due to its structural similarity with human serum albumin (HSA) and its low cost [76]. Three intrinsic fluorophores present in the protein are tryptophan, tyrosine, and phenylalanine residues. The intrinsic fluorescence of serum albumins is created by Trp alone, because Phe has a very low quantum yield and the fluorescence of Tyr is quenched if it is ionized or placed near an amino group, a carboxyl group, or a Trp. Thus the overall changes of intrinsic fluorescence intensity of serum albumins are related to the changes in the fluo-

Table 1
Crystal data and structure refinement for the polymeric complex.

	Complex
Formula	$C_{26}H_{24}N_4O_{10}.Zn_2.4(H_2O)$
Temperature/K	95 K
Crystal system	Monoclinic
Space group	*P 1 21/c 1*
a [Å]	18.4322(7)
b [Å]	8.4517(2)
c [Å]	19.2226(7)
α [°]	90
β [°]	104.960(3)
γ [°]	90
vol/Å^3	2893.07(17)
Z,Z'	4
D, g/cm^3	1.734
μ [mm^{-1}]	2.749
F(000)	1544.44
R(reflections)	0.0473(3563)
w*R2(reflections)*	0.1158(5183)

Table 2
Selected bond lengths (Å) and angles (°) for the polymeric complex.

Bond angles (°)		Bond lengths (Å)	
O1a,Zn1a,O2a	145.1(1)	Zn1a-O1a	2.027(3)
O1a,Zn1a,O4b	92.4(1)	Zn1a-O2a	2.069(4)
O1a,Zn1a,N1a	87.9(1)	Zn1a-O4b	1.959(4)
O1a,Zn1a,O3a	109.0(1)	Zn1a-N1a	2.039(4)
O2a,Zn1a,O4b	94.8(1)	Zn1a-O3a (polymeric)	2.020(3)
O2a,Zn1a,N1a	80.1(1)	Zn1b-O4a	2.001(3)
O2a,Zn1a,O3a	103.8(1)	Zn1b-O1b	2.048(3)
O4b,Zn1a,N1a	171.1(1)	Zn1b-O2b	2.218(3)
O4b,Zn1a,O3a	97.5(1)	Zn1b-N1b	2.036(4)
N1a,Zn1a,O3a	90.8(1)	Zn1b-O3b (polymeric)	1.975(3)
O4a,Zn1b,O1b	95.6(1)	O3a-Zn1a	2.020(3)
O4a,Zn1b,O2b	85.7(1)	O3b-Zn1b	1.975(3)
O4a,Zn1b,N1b	140.4(1)		
O4a,Zn1b,O3b	99.9(1)		
O1b,Zn1b,O2b	159.5(1)		
O1b,Zn1b,N1b	87.9(1)		
O1b,Zn1b,O3b	104.0(1)		
O2b,Zn1b,N1b	78.4(1)		
O2b,Zn1b,O3b	95.9(1)		
N1b,Zn1b,O3b	117.5(1)		
Zn1a,O1a,C1a	124.4(3)		
Zn1a,O2a,C9a	114.6(3)		
C9a,O3a,Zn1a	134.4(3)		
Zn1b,O4a,C13a	124.2(3)		
Zn1b,O1b,C1b	130.4(3)		
Zn1b,O2b,C9b	113.8(3)		
C9b,O3b,Zn1b	142.5(3)		
Zn1a,O4b,C13b	133.2(3)		
Zn1a,N1a,C7a	126.6(3)		
Zn1a,N1a,C8a	112.1(3)		
C7a,N1a,C8a	120.3(4)		
C11a,N2a,C12a	126.5(4)		
C11a,N2a,H1n2a	113(3)		
C12a,N2a,H1n2a	119(3)		
Zn1b,N1b,C7b	127.5(3)		
Zn1b,N1b,C8b	114.5(3)		

rescence intensity of Trp residue when small molecule is added to serum albumin [77–79]. Fluorescence emission is very sensitive to the environment and spectral shifts in the excitation and emission spectra have been observed during transferring the fluorophore between high and low polarity environment.

The effect of Zn(II) complex (5×10^{-5} M) (0-55 μL) on BSA (7.2×10^{-8} M) fluorescence intensity is shown in Fig. 3. It is obvious that serum albumin reveals strong fluorescence emission peak around 340 nm after excitation at 280 nm. By titration a fixed concentration of BSA with different amounts of complex, a remarkable quenching of BSA fluorescence emission peak with a hypsochromic shift due to the formation of a complex between the polymeric complex and BSA was observed [76]. The hypsochromic shift suggested that the microenvironment around tryptophan residues becomes slightly hydrophobic upon the interaction of polymeric complex with BSA [80].

The fluorescence quenching data are analyzed by the Stern–Volmer Eq. (1) [81].

$$\frac{F_0}{F} = 1 + K_{SV}[Q] = 1 + k_q \tau_0 [Q] \quad (1)$$

where F and F_0 are the fluorescence intensities in the presence and the absence of quencher, respectively. K_{SV} is the Stern-Volmer quenching constant, [Q] is the concentration of quencher, k_q is the bimolecular quenching constant, and τ_0 is the lifetime of the fluorophore in the absence of a quencher, which is 10^{-8} s for BSA [80].

K_{SV} values obtained from the plot of F_0/F *vs.* [Q]. The corresponding Stern-Volmer quenching constant was $K_{SV} = 3.9 \times 10^4$ (M^{-1}) and quenching rate constant was $k_q = 3.9 \times 10^{12}$ ($M^{-1}s^{-1}$) at 298 K. The linear Stern-Volmer plots indicated that Eq. (1) is applicable for the present systems (Fig. 4).

Two different mechanisms for fluorescence quenching are classified as dynamic quenching and static quenching. Dynamic quenching refers to the excited state when fluorophore and the quencher come into contact during the transient existence. The static quenching refers to fluorophore–quencher forming a ground state. In order to confirm the quenching mechanism of BSA by the polymeric complex, UV–Vis absorption spectra were recorded [82].

3.4. UV–Vis absorption studies

The UV–Vis spectral measurements can be used to distinguish the type of quenching mechanism i.e., static or dynamic quenching. Dynamic quenching causes no change in the absorption spectra because it effects on the excited state of the fluorophore. However, in the static quenching the ground-state complex formation results in changing of the absorption spectrum of the fluorophore [76].

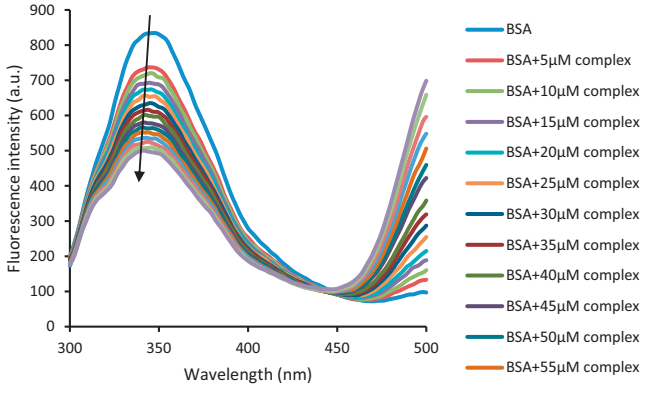

Fig. 3. Effect of Zn(II) complex on the fluorescence spectra of BSA ($\lambda_{Ex} = 280$), ([complex] = 5×10^{-5} M/[BSA] = 7.2×10^{-8} M): 1.0, 2.0, 3.1, 4.1, 5.1, 6.2, 7.2, 8.2, 9.2, 10.3, 11.3, 12.3, 13.4, 14.4, 15.4; (T = 298 K).

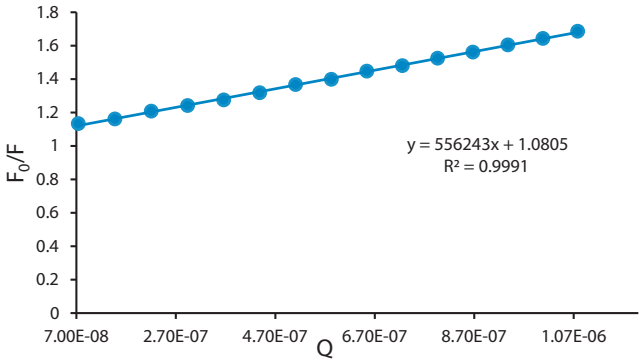

Fig. 4. The Stern–Volmer plot of the fluorescence titration of BSA (7.2×10^{-8} M) with complex (5×10^{-5} M) $\lambda_{Ex} = 280$ nm, $\lambda_{Em} = 345$ nm.

The absorption spectra of BSA (2×10^{-5} M) in the absence and presence of complex (8×10^{-4} M) (0–220 μL) are shown in Fig. S7 which displayed that the absorption intensity of BSA enhanced by addition the compound, with a slight blue shift [53]. This result suggested a static interaction between the complex and BSA due to the formation of a complex-BSA ground state system. The intrinsic binding constant, K_b was determined from the spectral titration data using Eq. (2) at four temperatures (293, 298, 303 and 308 K) (Figs. 5 & S8):

$$\frac{[complex]}{(\varepsilon a - -\varepsilon f)} = \frac{[complex]}{(\varepsilon b - -\varepsilon f)} + \frac{1}{Kb(\varepsilon b - -\varepsilon f)} \quad (2)$$

where [complex] is the concentration of complex, ε_a corresponds to the extinction coefficient observed ($A_{obsd}/[M]$), ε_f corresponds to the extinction coefficient of the free compound, ε_b is the extinction coefficient of the compound when fully bound to BSA, and K_b is the intrinsic binding constant. The ratio of slope to intercept in the plot of [complex]/($\varepsilon_a - \varepsilon_f$) versus [complex] gave the values of K_b (Fig. 6) which are presented in Table 3.

The different quenching mechanisms are usually classified as either dynamic or static interaction, which can be distinguished by their different dependence on temperature and viscosity, or by lifetime measurements. Dynamic interaction mainly depends on diffusion. Higher temperatures will result in faster diffusion and hence higher dynamic interaction constants. In the case of static interaction, a complex is formed between bio-macromolecule and the quencher in the ground state. Increasing of temperature result in the dissociation of weakly bound complexes, and therefore, the values of the static interaction constants are expected to be smaller [83]. The K_b at different temperatures in Table 3 suggested a static quenching pathway, because the K_b decreased with increasing the temperature.

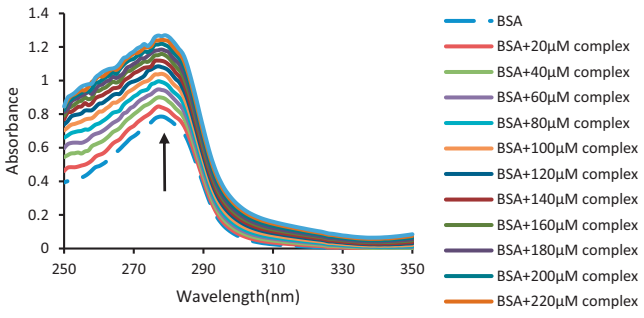

Fig. 5. Titration of BSA (dotted line) (2×10^{-5} M) with various concentrations of complex (8×10^{-4} M) at 293 K.

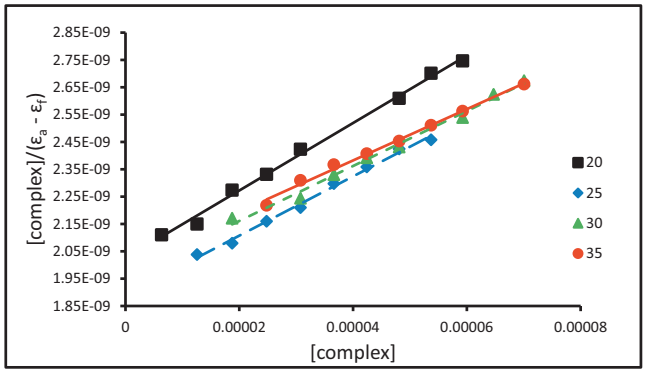

Fig. 6. The plot of [complex]/($\varepsilon_a - \varepsilon_f$) versus [complex] at 20, 25, 30 and 35 °C.

3.5. Thermodynamic parameters and binding modes

The binding of metal complexes to BSA were characterized classically through spectrophotometric titrations, by following the changes in absorption spectra. Protein–drug binding is included of hydrophobic interactions, electrostatic interactions, van der Waals forces and hydrogen bonds. The binding mode can be determined by analyzing the thermodynamic parameters such as free energy, enthalpy and entropy, which serve the main evidence for confirming the binding mode. The ΔH and ΔS values were calculated from Van't Hoff Eq. (3) [80,84]:

$$\ln Kb = -\frac{H}{RT} + \frac{S}{R} \quad (3)$$

where K_b is defined as the binding constant at special temperatures and R is the gas constant. Eq. (4) was used to calculate Free energy changes (ΔG) at different temperatures [84]:

$$G = H - TS \quad (4)$$

Thermodynamic parameters determined from the linear Van't Hoff plot (Fig. S9) are presented in Table 3. The ΔH and ΔS values suggest that the binding between BSA and complex was exothermic and entropy-driven process. The negative value of ΔG indicated that the interaction process was spontaneous. According to the criteria set up by Ross and Subramanian [85], the negative ΔH and positive ΔS values indicated that electrostatic forces play an important role in the complex-BSA binding interaction [80].

3.6. Binding stoichiometry

For determination the average aggregation number of BSA, ⟨J⟩, Eq. (5) was used.

$$1 - \frac{F}{F_0} = \langle J \rangle \frac{[Q]}{[BSA]_0} \quad (5)$$

The linear plots have been presented. The slopes (⟨J⟩) (Fig. S10) with $J = 0.0015 < 1$ showed that the complex did not aggregate on BSA molecules and the stoichiometry for complex-BSA system was 1:1.

3.7. Binding constants and the number of binding sites

For static quenching interaction, the fluorescence intensity data can also be used to analyze the apparent binding constant (K_b) and the number of binding sites (n) for the complex and BSA system by Eq. (6) [82]:

$$\log\left(\frac{F_0 - F}{F}\right) = \log K_b + n\log[Q] \quad (6)$$

where K_b is the binding constant of the compound with BSA, n is the number of binding sites and [Q] is the concentration of quencher. From the plot of log [($F_0 - F$)/F] *vs.* log [Q], the binding constant ($K_b = 8.8 \times 10^3\ (M^{-1})$) and the number of binding sites (n = 0.339) were calculated (Fig. S11). The value of n was approximately equal to 1, suggested that there was only one binding site for the complex on BSA [82].

3.8. Site-selective binding of complex on BSA

Bovine serum albumin has two main sites for binding to drugs: (i) site I of BSA in which tryptophan residue is bound to drugs and (ii) site II in which tyrosine is located and capable to accept the binding of drugs. In order to identify the preference of the binding sites by drugs, displacement experiments were performed with phenylbutazone and ibuprofen as site markers, because site I of BSA showed affinity for warfarin, phenylbutazone, etc., whereas site II was well suited for ibuprofen, diazepam, fluofenamic acid, etc. [86] The emission spectra of a mixture of complex (5×10^{-5} M) (0–45 μL), BSA (7.2×10^{-8} M) and site marker (1.8×10^{-5} M) were measured to identify the binding site. The spectra showed that the quenching of BSA in the presence of ibuprofen was smaller than in its absence (Fig. 7). The calculated binding constants (Table 4) revealed that by addition of ibuprofen, the binding constant of complex-BSA system decreased while it remained almost constant with the addition of phenyl butazone. These results revealed that the complex was displaced from the binding site by ibuprofen, thus the complex were mainly located in the region of site II (subdomain IIIA) in BSA.

3.9. Energy transfer and binding distance between complex and BSA

Proximity and angular orientation of fluorophores can be estimated by FRET (Fluorescence resonance energy transfer) which is a nondestructive spectroscopic method. FRET has been nominated as "spectroscopic ruler". Because by this method the molecular distance between the complex and protein systems can be measured. Calculating the molecular distance has been done by overlapping the fluorescence emission band of donor with excitation band of acceptor. If these two band overlap with each other, it means that they are within 2–8 nm distance from each other [87,88]. Thus the effective energy transfer from donor to acceptor can happen. In the FRET method fluorophore nominated as donor and it must be enough overlap between the fluorescence emission spectrum of the donor and UV–Vis absorption spectrum of the acceptor [89].

Energy transfer in the Förster theory is affected by two parameters: the distance between acceptor and donor and the critical

Table 3
Apparent binding constant and relative thermodynamic parameters for the interaction of complex with BSA at different temperatures.

T (K)	K_b (M^{-1})	R^2	ΔH (kJ mol^{-1})	ΔG (kJ mol^{-1})	ΔS (J mol^{-1} K^{-1})
293	$(6.1 \pm 0.1) \times 10^3$	0.9909	−13.4 ± 0.9	−21.25 ± 0.11	26.8 ± 3.0
298	$(5.7 \pm 0.2) \times 10^3$	0.9937		−21.39 ± 0.13	
303	$(5.1 \pm 0.3) \times 10^3$	0.9916		−21.52 ± 0.14	
308	$(4.7 \pm 0.2) \times 10^3$	0.9932		−21.65 ± 0.12	

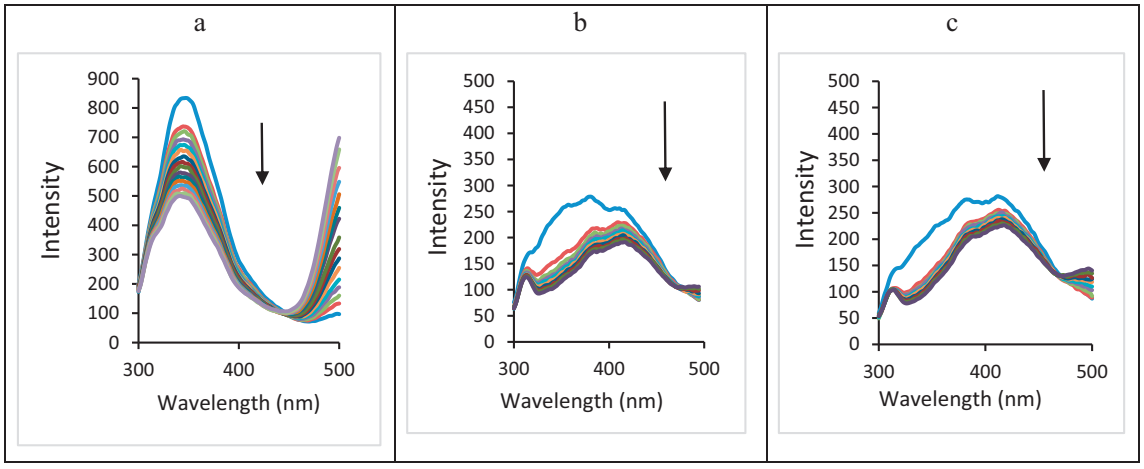

Fig. 7. Quenching effect of BSA (7.2×10^{-8} M) binding to complex (5×10^{-5} M) (0–45 μL) in the a) absence of site marker, b) presence of phenyl butazone (1.8×10^{-5} M) and c) presence of ibuprofen (1.8×10^{-5} M).

Table 4
Binding constants of competitive experiments of complex-BSA system.

Site marker	K_b (M^{-1})	R^2
Without	$8.8 \pm 0.1 \times 10^3$	0.9923
Ibuprofen	$0.8 \pm 0.3 \times 10^3$	0.9911
Phenyl butazone	$2.9 \pm 0.2 \times 10^3$	0.9965

distance of energy transfer (R_0), which can be calculated by using Eq. (7):

$$E = \frac{R_0^6}{R_0^6 + r^6} = 1 - \frac{F}{F_0} \quad (7)$$

where F and F_0 are the fluorescence intensities of biomolecule in the presence and absence of quencher, r the donor–acceptor distance and R_0 the critical distance where the transfer efficiency is 50%:

$$R_0^6 = 8.8 \times 10^{-25} K^2 N^{-4} \Phi J \quad (8)$$

where K_2 is defined as spatial orientation factor this factor is related to the geometry of the donor and acceptor, and a random orientation is defined by $K^2 = 2/3$ in fluid solution, N is the averaged refracted index of the medium is defined by N in the wavelength range where spectral overlap is significant, but for the average refracted index of water and organics N = 1.336 is used, the fluorescence quantum yield of the donor is shown by Φ, and Φ = 0.118 is a special figure for the fluorescence quantum yield of tryptophan [89], and finally the effect of the spectral overlap between the emission spectrum of the donor and the absorption spectrum of the acceptor is defined by J, which can be calculated by using Eq. (9):

$$J = \frac{\int_0^\infty F(\lambda)\varepsilon(\lambda)\lambda^4 d\lambda}{\int_0^\infty F(\lambda) d\lambda} \quad (9)$$

In this Equation F(λ) is nominated as the corrected fluorescence intensity of the donor where the wavelength range is varied from λ to (l + Δλ) and ε(λ) is the molar extinction coefficient of the acceptor at wavelength λ.

As shown in Fig. 8, the emission spectrum of BSA (7.2×10^{-8} M) overlaps with the absorption spectrum of the complex (5×10^{-5} M) in the wavelength range from 300 to 470 nm. This considerable overlap forms the basis of FRET. Thus, the Förster's non-radiative energy transfer theory can be used to determine the distance between the amino acid residues on protein and the complex in the binding site [56]. The corresponding results are shown in Table 5. The value of r = 2.14 nm is less than 8 nm, and

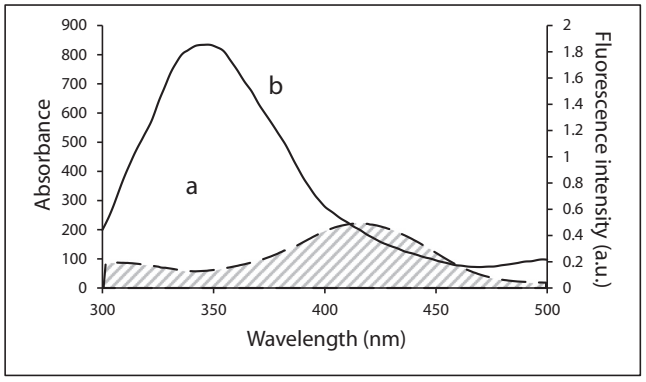

Fig. 8. Spectral overlap of the absorption of complex (5×10^{-5} M) (a) with the BSA (7.2×10^{-8} M) fluorescence spectrum (b).

Table 5
Energy transfer parameters for the interaction of metal complex with BSA.

R_0 (nm)	r (nm)	J (cm^3 L mol^{-1})	E
2.01	2.14	2.59×10^{-15}	0.41

$0.5R_0 < r < 1.5R_0$, indicating the energy transfer from BSA to the complex occurs with high probability [90–92].

3.10. Synchronous fluorescence spectroscopic studies

Three amino acids: tyrosine, tryptophan and phenylalanine residues cause the fluorescence of BSA which is very sensitive to the microenvironment of these chromophores. In the synchronous fluorescence spectroscopy the conformational changes of BSA in the presence of the complex can be investigated [93]. In synchronous fluorescence spectroscopy, the different nature of chromophores, is shown by the difference between excitation and emission wavelengths ($\Delta\lambda = \lambda_{em} - \lambda_{ex}$) of tryptophan and tyrosine residue. The large Δλ (60 nm) are ascribed to the fluorescence of tryptophan while the small Δλ (15 nm) for tyrosine residue [94]. It is worthy to note that the maxima of emission spectra of the tryptophan and tyrosine residues in proteins are related to the polarity of their surroundings [93]. In this regard increasing polarity of the surrounding environment and/or lower hydrophobicity of it and/or more loose structure of BSA can all cause the red shift

of the maximum emission wavelength in synchronous fluorescence [89]. The effect of complex (5×10^{-5} M) (0–40 μL) on the synchronous fluorescence spectra of BSA (7.2×10^{-8} M) is shown in Fig. 9. With increasing the concentrations of complex, the synchronous fluorescence spectra at $\Delta\lambda = 15$ nm for BSA displayed a decrease in fluorescence intensity at 282 nm with slight blue shift of 1–2 nm and at $\Delta\lambda = 60$ nm exhibited a decrease in fluorescence intensity at 280 nm without any appreciable shift in the position of the band.

Quenching of the fluorescence of BSA with both $\Delta\lambda$ indicated that complex could bind to tyrosine and tryptophan residues simultaneously. As it was mentioned previously, the maximum emission wavelength of tyrosine residues had a blue shift but no obvious wavelength shift of tryptophan residues was observed, which suggested the decreasing of the polarity around tyrosine residues and increasing the hydrophobicity, but it was assumed that the polarity around tryptophan residues had no remarkable change during the binding process [89].

3.11. Inhibitory effects of the complex on various cancer cell lines

The anticancer properties of complex have been already proved [95–99]. Water solubility is a main character of a metal complex when it considers as a drug candidate. Providing some ionic groups on the metal complexes increase their hydrophilicity and water solubility. Some ionic groups like PPh_3^+ also increase the lipophilicity of complex and accelerate passing through biological membranes.

By considering the polymeric complex, it is clear that lipophilic parts were provided in the polymeric complex (aromatic rings) and hydrophilic parts were also provided (glycine bridge and water molecules which coordinated to the central metal) thus this complex can easily pass through biological membrane and reveal anticancer activity. In the current study the synthetic complex was screened for its cytotoxicity activities on A549, Jurkat and Raji cell lines as the target. The cell lines were incubated in the presence of increasing concentrations of the complex for 48 h, and then cytotoxicity was measured. In Figs. S12–14, the inhibitory effects of the complex against cancer cell lines are shown. Generally, the complex showed strong growth inhibitory activity against the cell lines. In order to compare the cytotoxic effects of the complex, the IC_{50} values were determined. IC_{50} value is defined as the concentration of a compound where 50% of the cell growth is inhibited. In Table 6, based on the IC_{50} values, the cytotoxic activity of complex for A549, Jurkat and Raji cell lines are shown. The complex had a stronger activity against leukemia lymphoma cells (IC_{50}, 7.3 μg/mL for Jurkat and 9.3 μg/mL for Raji) compared to A549 (IC_{50}, 93.6 μg/mL). The IC_{50} values of *cisplatin* for A549 cell line was 79.4 μg/mL, 25 μg/mL for Jurkat and 30 μg/mL for Raji cells.

Table 6
The Inhibitory concentration (IC) 50% for the effects of the complexes on various cell lines.

IC_{50}(μg/ml)		
A549	Jurkat	Ragi
93.6 ± 4	7.3 ± 1	9.3 ± 3

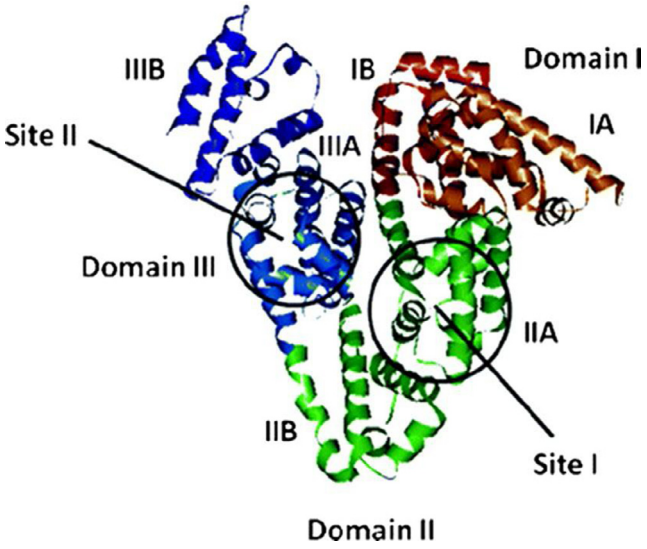

Fig. 10. The structure of BSA.

3.12. Molecular docking study

The BSA molecule includes three homologous domains: domain I (residues 1–195), II (196–383) and III (384–585) that are divided into nine loops (L1–L9) and connected to each other via 17 disulfide bonds. Each domain is composed of two sub-domains (A and B) (Fig. 10). The presence of two tryptophan residues (Trp-134 and Trp-212) makes an intrinsic fluorescence in BSA molecule. On the surface of subdomain IB, Trp-134 is located and within the hydrophobic binding pocket of subdomain IIA, Trp-212 is

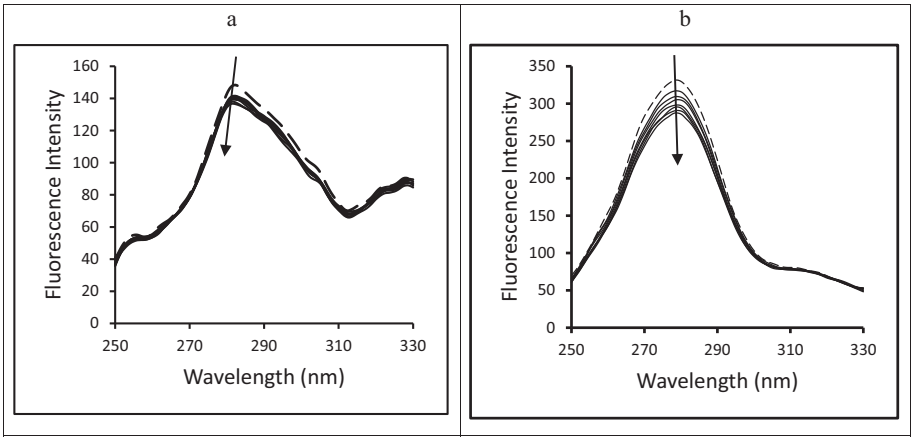

Fig. 9. Synchronous fluorescence spectra of BSA (7.2×10^{-8} M) with $\Delta\lambda = 15$ nm (a) and $\Delta\lambda = 60$ nm (b) in the absence (dashed lines) and presence (solid lines) of complex (5×10^{-5} M) (0–40 μL).

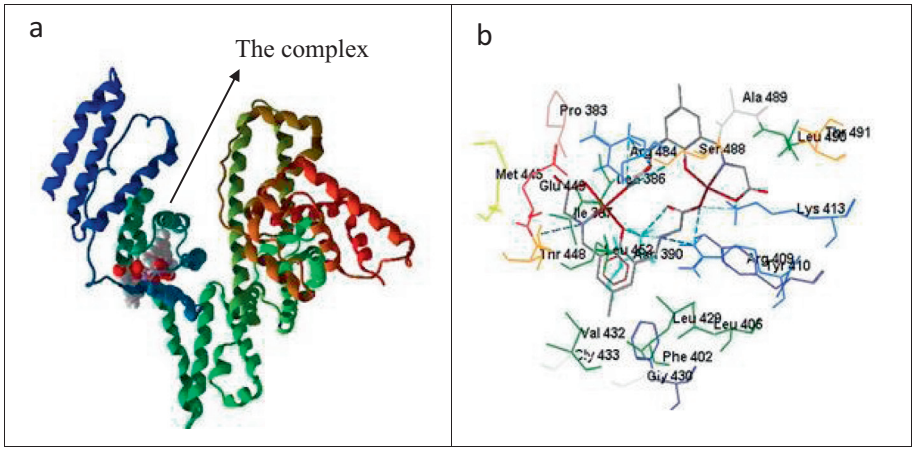

Fig. 11. a) Position of the complex docked in the binding site. b) The amino acid residues which surrounding the complex.

located. In the present study, the MVD program was used to obtain the binding mode of the complex at the active site of BSA. As can be observed in the docking results, the complex preferred the binding pocket of site II (subdomain IIIA). Additionally, there are some specific hydrogen bonds which are due to the presence of several polar residues in the proximity of the protein and can play an important role in binding of the complex to BSA. In fact, hydrogen bonding can be formed between the O, N, H of a Schiff base complex and the amino acid residues of BSA (Fig. 11). On the basis of these results, it can be suggested that the formation of hydrogen bonds stabilizes the complex–BSA composition. Also, the energy for the binding of complex to BSA was found to be −134.037. These results are very close to those obtained from the above-mentioned experimental method. Amino-acid residues are involved in the complex–BSA interactions and binding energy for the best selected docking positions are Ala489, Arg409, Arg484, Asn390, Gln384, Glu382, Glu449, Gly430, Gly433, Ile387, Leu386, Leu406, Leu429, Leu452, Leu490, Lys413, Met445, Phe402, Phe487, Pro383, Pro485, Ser488, Thr448, Thr491, Tyr410, Val432.

4. Conclusion

A new water soluble polymeric complex was synthesized and characterized by elemental analysis, FT-IR, ^{1}H NMR and UV–Vis spectroscopy, and X-ray structure analysis. The binding interaction of this complex with BSA was investigated by spectroscopic methods. Experimental results suggested that this complex could bind to the serum albumins, and the corresponding quenching rate constants were calculated by Stern-Volmer equation. Experimental results also showed quenching of fluorescence emission intensity with a hypsochromic shift during the binding process.

Competitive experiments also showed that the complex was bound to site II of serum albumin. Based on the Förster energy transfer theory, the transfer efficiency of energy and the distance between the complex and proteins were obtained.

From the synchronous fluorescence spectrum, it was concluded that the interaction of complex with albumins did not change the conformation of tryptophan microenvironment, while the hydrophobicity near the tyrosine residues was changed.

Thermodynamic results indicated that the binding process is exothermic for the complex and essentially entropy-driven. This suggested that electrostatic forces play an important role in the binding reaction. The high affinity of albumins for the complex was clearly evidenced by ΔG values which clarified the role of albumins as endogenous carrier for this complex in the body, which could be a useful guideline for further drug design. The values of K_b at different temperatures suggested a static quenching pathway, because the K_b decreased with increasing the temperature.

Finally, the mentioned complex was also screened for its anticancer activities with Jurkat human T cell leukemia, Raji Burkitt's lymphoma and A549 lung carcinoma cell lines as the target. According to IC_{50} values, the results indicated that this complex can be a potential anticancer agent.

Acknowledgements

We are grateful to the Shiraz university research council for its financial support. The crystallographic part was supported by the project 14-03276S of the Czech Science Foundation using instruments of the ASTRA lab established within the Operation program Prague Competitiveness – project CZ.2.16/3.1.00/24510.

Appendix A. Supplementary data

CCDC 1520739 contains the supplementary crystallographic data for this paper. These data can be obtained free of charge from The Cambridge Crystallographic Data Centre via www.ccdc.cam.ac.uk/data_request/cif. Supplementary data associated with this article can be found, in the online version, at http://dx.doi.org/10.1016/j.ica.2017.05.066.

References

[1] B.F. Hoskins, R. Robson, Infinite polymeric frameworks consisting of three dimensionally linked rod-like segments, J. Am. Chem. Soc. 111 (1989) 5962–5964.
[2] A. Messai, D. Bilge, M. Bilge, C. Parlak, New Cu (II) coordination polymer by chiral tridentate Schiff base ligand, J. Mol. Struct. 1137 (2017) 349–353.
[3] S.S.-Y. Chui, S.M.-F. Lo, J.P. Charmant, A.G. Orpen, I.D. Williams, A chemically functionalizable nanoporous material [Cu3 (TMA) 2 (H2O) 3] n, Science 283 (1999) 1148–1150.
[4] M. Eddaoudi, H. Li, O. Yaghi, Highly porous and stable metal-organic frameworks: structure design and sorption properties, J. Am. Chem. Soc. 122 (2000) 1391–1397.
[5] C.J. Kepert, M.J. Rosseinsky, Zeolite-like crystal structure of an empty microporous molecular framework, Chem. Commun. 375–376 (1999).
[6] M. Kondo, T. Yoshitomi, H. Matsuzaka, S. Kitagawa, K. Seki, Three-Dimensional Framework with Channeling Cavities for Small Molecules: {[M2(4,4′-bpy)3 (NO3)4]·xH$_2$O}n (M = Co, Ni, Zn), Angew. Chem. Int. Ed. Engl. 36 (1997) 1725–1727.
[7] H. Li, M. Eddaoudi, M. O'Keeffe, O.M. Yaghi, Design and synthesis of an exceptionally stable and highly porous metal-organic framework, Nature 402 (1999) 276–279.
[8] J.-R. Li, J. Sculley, H.-C. Zhou, Metal–organic frameworks for separations, Chem. Rev. 112 (2011) 869–932.
[9] L.J. Murray, M. Dincă, J.R. Long, Hydrogen storage in metal–organic frameworks, Chem. Soc. Rev. 38 (2009) 1294–1314.

[10] S.I. Noro, S. Kitagawa, M. Kondo, K. Seki, A new, methane adsorbent, porous coordination polymer [{CuSiF6 (4, 4′-bipyridine) 2} n], Angew. Chem. Int. Ed. 39 (2000) 2081–2084.
[11] O.M. Yaghi, G. Li, H. Li, Selective binding and removal of guests in a microporous metal–organic framework, Nature 378 (1995) 703–706.
[12] S. Achmann, G. Hagen, J. Kita, I.M. Malkowsky, C. Kiener, R. Moos, Metal-organic frameworks for sensing applications in the gas phase, Sensors 9 (2009) 1574–1589.
[13] M. Allendorf, C. Bauer, R. Bhakta, R. Houk, Luminescent metal–organic frameworks, Chem. Soc. Rev. 38 (2009) 1330–1352.
[14] L.E. Kreno, K. Leong, O.K. Farha, M. Allendorf, R.P. Van Duyne, J.T. Hupp, Metal–organic framework materials as chemical sensors, Chem. Rev. 112 (2011) 1105–1125.
[15] K. Biradha, C. Seward, M.J. Zaworotko, Helical coordination polymers with large chiral cavities, Angew. Chem. Int. Ed. 38 (1999) 492–495.
[16] S.-H. Cho, B. Ma, S.T. Nguyen, J.T. Hupp, T.E. Albrecht-Schmitt, A metal–organic framework material that functions as an enantioselective catalyst for olefin epoxidation, Chem. Commun. 2563–2565 (2006).
[17] M. Fujita, Y.J. Kwon, S. Washizu, K. Ogura, Preparation, clathration ability, and catalysis of a two-dimensional square network material composed of cadmium (II) and 4, 4'-bipyridine, J. Am. Chem. Soc. 116 (1994) 1151–1152.
[18] T. Sawaki, T. Dewa, Y. Aoyama, Immobilization of soluble metal complexes with a hydrogen-bonded organic network as a supporter. A simple route to microporous solid Lewis acid catalysts, J. Am. Chem. Soc. 120 (1998) 8539–8540.
[19] K. Schlichte, T. Kratzke, S. Kaskel, Improved synthesis, thermal stability and catalytic properties of the metal-organic framework compound Cu 3 (BTC) 2, Microporous Mesoporous Mater. 73 (2004) 81–88.
[20] J.S. Seo, D. Whang, H. Lee, S. Im Jun, J. Oh, Y.J. Jeon, K. Kim, A homochiral metal–organic porous material for enantioselective separation and catalysis, Nature 404 (2000) 982–986.
[21] J.M. Tanski, P.T. Wolczanski, Covalent titanium aryldioxy one-, two-, and three-dimensional networks and their examination as Ziegler-Natta catalysts, Inorg. Chem. 40 (2001) 2026–2033.
[22] M. Yoon, R. Srirambalaji, K. Kim, Homochiral metal–organic frameworks for asymmetric heterogeneous catalysis, Chem. Rev. 112 (2011) 1196–1231.
[23] H. Guo, Y. Zhu, S. Qiu, J.A. Lercher, H. Zhang, Coordination modulation induced synthesis of nanoscale Eu1-xTbx-metal-organic frameworks for luminescent thin films, Adv. Mater. 22 (2010) 4190–4192.
[24] H.C. Streit, M. Adlung, O. Shekhah, X. Stammer, H.K. Arslan, O. Zybaylo, T. Ladnorg, H. Gliemann, M. Franzreb, C. Wöll, Surface-anchored MOF-based photonic antennae, Chem. Phys. Chem. 13 (2012) 2699–2702.
[25] J.L. Atwood, Kagome lattice: a molecular toolkit for magnetism, Nat. Mater. 1 (2002) 91–92.
[26] G.J. Halder, C.J. Kepert, B. Moubaraki, K.S. Murray, J.D. Cashion, Guest-dependent spin crossover in a nanoporous molecular framework material, Science 298 (2002) 1762–1765.
[27] D. Maspoch, D. Ruiz-Molina, J. Veciana, Magnetic nanoporous coordination polymers, J. Mater. Chem. 14 (2004) 2713–2723.
[28] D. Maspoch, D. Ruiz-Molina, K. Wurst, N. Domingo, M. Cavallini, F. Biscarini, J. Tejada, C. Rovira, J. Veciana, A nanoporous molecular magnet with reversible solvent-induced mechanical and magnetic properties, Nat. Mater. 2 (2003) 190–195.
[29] B. Moulton, J. Lu, R. Hajndl, S. Hariharan, M.J. Zaworotko, Crystal engineering of a nanoscale Kagomé lattice, Angew. Chem. Int. Ed. 41 (2002) 2821–2824.
[30] P.K. Goswami, M. Singh, R. Thaimattam, A. Ramanan, Extending the supramolecular synthon concept in flexible polyaminocarboxylate based coordination polymers, Cryst. Eng. Comm. 15 (2013) 9787–9797.
[31] Y.-T. Li, Z.-Q. Liu, Z.-Y. Wu, One-dimensional copper (II) coordination polymers bridged both by μ-trans-oxamidates and phenyldicarboxylates: synthesis, crystal structure and DNA binding studies, J. Inorg. Biochem. 102 (2008) 1790–1797.
[32] S. Noro, J. Mizutani, Y. Hijikata, R. Matsuda, H. Sato, S. Kitagawa, K. Sugimoto, Y. Inubushi, K. Kubo, T. Nakamura, Porous coordination polymers with ubiquitous and biocompatible metals and a neutral bridging ligand, Nat. Commun. 6 (2015) 5851.
[33] S. Emami, S.J. Hosseinimehr, S.M. Taghdisi, S. Akhlaghpoor, Kojic acid and its manganese and zinc complexes as potential radioprotective agents, Bioorg. Med. Chem. Lett. 17 (2007) 45–48.
[34] Q. Huang, Z. Pan, P. Wang, Z. Chen, X. Zhang, H. Xu, Zinc (II) and copper (II) complexes of β-substituted hydroxylporphyrins as tumor photosensitizers, Bioorg. Med. Chem. Lett. 16 (2006) 3030–3033.
[35] A. Nakayama, M. Hiromura, Y. Adachi, H. Sakurai, Molecular mechanism of antidiabetic zinc–allixin complexes: regulations of glucose utilization and lipid metabolism, J. Biol. Inorg. Chem. 13 (2008) 675–684.
[36] H. Sakurai, Y. Yoshikawa, H. Yasui, Current state for the development of metallopharmaceutics and anti-diabetic metal complexes, Chem. Soc. Rev. 37 (2008) 2383–2392.
[37] Z.H. Chohan, M. Arif, M. Sarfraz, Metal-based antibacterial and antifungal amino acid derived Schiff bases: their synthesis, characterization and in vitro biological activity, Appl. Organomet. Chem. 21 (2007) 294–302.
[38] A. Katiyar, V.P. Singh, Synthesis, structural studies and bio-activity of Mn (II), Co (II), Ni (II), Cu (II) and Zn (II) complexes with p-amino acetophenone salicyloyl hydrazone, J. Coord. Chem. 61 (2008) 3200–3212.
[39] M.T. Kaczmarek, R. Jastrząb, E. Hołderna-Kędzia, W. Radecka-Paryzek, Self-assembled synthesis, characterization and antimicrobial activity of zinc (II) salicylaldimine complexes, Inorg. Chim. Acta 362 (2009) 3127–3133.
[40] D. Majumdar, M.S. Babu, S. Das, J.K. Biswas, M. Mondal, S. Hazra, Synthesis, X-ray crystal structure, photo luminescent property, antimicrobial activities and DFT computational study of Zn (II) coordination polymer derived from multisite N, O donor Schiff base ligand (H 2 L 1), J. Mol. Struct. 1138 (2017) 161–171.
[41] A. Arbuse, M. Font, M.A. Martínez, X. Fontrodona, M.J. Prieto, V. Moreno, X. Sala, A. Llobet, DNA-cleavage induced by new macrocyclic Schiff base dinuclear Cu (I) complexes containing pyridyl pendant arms, Inorg. Chem. 48 (2009) 11098–11107.
[42] F. Arjmand, F. Sayeed, Synthesis, characterization and DNA-binding studies of mono and heterobimetallic complexes CuSn2/ZnSn2 and their DNA cleavage activity, J. Mol. Struct. 965 (2010) 14–22.
[43] A. Paul, R.K. Gupta, M. Dubey, G. Sharma, B. Koch, G. Hundal, M.S. Hundal, D.S. Pandey, Potential apoptosis inducing agents based on a new benzimidazole schiff base ligand and its dicopper (II) complex, RSC Adv. 4 (2014) 41228–41236.
[44] V.K. Singh, R. Kadu, H. Roy, P. Raghavaiah, S.M. Mobin, Phenolate based metallomacrocyclic xanthate complexes of Co II/Cu II and their exclusive deployment in [2:2] binuclear N, O-Schiff base macrocycle formation and in vitro anticancer studies, Dalton Trans. 45 (2016) 1443–1454.
[45] K. Suntharalingam, A.J. White, R. Vilar, Two metals are better than one: investigations on the interactions between dinuclear metal complexes and quadruplex DNA, Inorg. Chem. 49 (2010) 8371–8380.
[46] Q. Jiang, N. Xiao, P. Shi, Y. Zhu, Z. Guo, Design of artificial metallonucleases with oxidative mechanism, Coord. Chem. Rev. 251 (2007) 1951–1972.
[47] J. Chen, X. Wang, Y. Shao, J. Zhu, Y. Zhu, Y. Li, Q. Xu, Z. Guo, A trinuclear copper (II) complex of 2, 4, 6-tris (di-2-pyridylamine)-1, 3, 5-triazine shows prominent DNA cleavage activity, Inorg. Chem. 46 (2007) 3306–3312.
[48] Y.-G. Fang, J. Zhang, S.-Y. Chen, N. Jiang, H.-H. Lin, Y. Zhang, X.-Q. Yu, Chiral multinuclear macrocyclic polyamine complexes: synthesis, characterization and their interaction with plasmid DNA, Bioorg. Med. Chem. 15 (2007) 696–701.
[49] J.L. García-Giménez, G. Alzuet, M. González-Álvarez, A. Castiñeiras, M. Liu-González, J. Borrás, A dinuclear copper (II) complex with adeninate bridge ligands and prominent DNA cleavage activity. Structural and spectroscopic characterization and magnetic properties, Inorg. Chem. 46 (2007) 7178–7188.
[50] K.J. Humphreys, K.D. Karlin, S.E. Rokita, Efficient and specific strand scission of DNA by a dinuclear copper complex: comparative reactivity of complexes with linked tris (2-pyridylmethyl) amine moieties, J. Am. Chem. Soc. 124 (2002) 6009–6019.
[51] C. Tu, Y. Shao, N. Gan, Q. Xu, Z. Guo, Oxidative DNA strand scission induced by a trinuclear copper (II) complex, Inorg. Chem. 43 (2004) 4761–4766.
[52] Y. Zhao, J. Zhu, W. He, Z. Yang, Y. Zhu, Y. Li, J. Zhang, Z. Guo, Oxidative DNA cleavage promoted by multinuclear copper complexes: activity dependence on the complex structure, Chem. Eur. J. 12 (2006) 6621–6629.
[53] D.S. Raja, N.S. Bhuvanesh, K. Natarajan, A novel water soluble ligand bridged cobalt (II) coordination polymer of 2-oxo-1, 2-dihydroquinoline-3-carbaldehyde (isonicotinic) hydrazone: evaluation of the DNA binding, protein interaction, radical scavenging and anticancer activity, Dalton Trans. 41 (2012) 4365–4377.
[54] S. Rojas, P.S. Wheatley, E. Quartapelle-Procopio, B. Gil, B. Marszalek, R.E. Morris, E. Barea, Metal–organic frameworks as potential multi-carriers of drugs, Cryst. Eng. Comm. 15 (2013) 9364–9367.
[55] M. Anjomshoa, H. Hadadzadeh, M. Torkzadeh-Mahani, S.J. Fatemi, M. Adeli-Sardou, H.A. Rudbari, V.M. Nardo, A mononuclear Cu (II) complex with 5, 6-diphenyl-3-(2-pyridyl)-1, 2, 4-triazine: synthesis, crystal structure, DNA-and BSA-binding, molecular modeling, and anticancer activity against MCF-7, A-549, and HT-29 cell lines, Eur. J. Med. Chem. 96 (2015) 66–82.
[56] H. Farrokhpour, H. Hadadzadeh, F. Darabi, F. Abyar, H.A. Rudbari, T. Ahmadi-Bagheri, A rare dihydroxo copper (II) complex with ciprofloxacin; a combined experimental and ONIOM computational study of the interaction of the complex with DNA and BSA, RSC Adv. 4 (2014) 35390–35404.
[57] P. Kandagal, S. Ashoka, J. Seetharamappa, S. Shaikh, Y. Jadegoud, O. Ijare, Study of the interaction of an anticancer drug with human and bovine serum albumin: spectroscopic approach, J. Pharm. Biomed. Anal. 41 (2006) 393–399.
[58] R.R. Kumar, M.K.M. Subarkhan, R. Ramesh, Synthesis and structure of nickel (II) thiocarboxamide complexes: effect of ligand substitutions on DNA/protein binding, antioxidant and cytotoxicity, RSC Adv. 5 (2015) 46760–46773.
[59] W.-J. Lian, X.-T. Wang, C.-Z. Xie, H. Tian, X.-Q. Song, H.-T. Pan, X. Qiao, J.-Y. Xu, Mixed-ligand copper (ii) Schiff base complexes: the role of the co-ligand in DNA binding, DNA cleavage, protein binding and cytotoxicity, Dalton Trans. 45 (2016) 9073–9087.
[60] V. Rajendiran, R. Karthik, M. Palaniandavar, H. Stoeckli-Evans, V.S. Periasamy, M.A. Akbarsha, B.S. Srinag, H. Krishnamurthy, Mixed-ligand copper (II)-phenolate complexes: effect of coligand on enhanced DNA and protein binding, DNA cleavage, and anticancer activity, Inorg. Chem. 46 (2007) 8208–8221.
[61] E. Sundaravadivel, S. Vedavalli, M. Kandaswamy, B. Varghese, P. Madankumar, DNA/BSA binding, DNA cleavage and electrochemical properties of new multidentate copper (II) complexes, RSC Adv. 4 (2014) 40763–40775.
[62] A. Tarushi, C.P. Raptopoulou, V. Psycharis, A. Terzis, G. Psomas, D.P. Kessissoglou, Zinc (II) complexes of the second-generation quinolone

antibacterial drug enrofloxacin: structure and DNA or albumin interaction, Bioorg. Med. Chem. 18 (2010) 2678–2685.
[63] K. Zheng, F. Liu, X.-M. Xu, Y.-T. Li, Z.-Y. Wu, C.-W. Yan, Synthesis, structure and molecular docking studies of dicopper (II) complexes bridged by N-phenolato-N′-[2-(dimethylamino) ethyl] oxamide: the influence of terminal ligands on cytotoxicity and reactivity towards DNA and protein BSA, New J. Chem. 38 (2014) 2964–2978.
[64] S. Kathiresan, S. Mugesh, M. Murugan, F. Ahamed, J. Annaraj, Mixed-ligand copper (II)-phenolate complexes: structure and studies on DNA/protein binding profiles, DNA cleavage, molecular docking and cytotoxicity, RSC Adv. 6 (2016) 1810–1825.
[65] W.E. Klopfenstein, Enthalpy change of binding lysolecithin to serum albumin, Biochim. Biophys. Acta 181 (1969) 323–325.
[66] D. Biswal, N.R. Pramanik, S. Chakrabarti, M.G. Drew, B. Sarkar, M.R. Maurya, S. K. Mukherjee, P. Chowdhury, New polymeric, dimeric and mononuclear dioxidomolybdenum (vi) complexes with an ONO donor ligand: crystal structures, DFT calculations, catalytic performance and protein binding study of the ligand, New J. Chem. (2017).
[67] C.N. Verani, E. Rentschler, T. Weyhermüller, E. Bill, P. Chaudhuri, Exchange coupling in a bis (heterodinuclear)[Cu II Ni II] 2 and a linear heterotrinuclear complex Co III Cu II Ni II. Synthesis, structures and properties, J. Chem. Soc., Dalton Trans. (2000) 251–258.
[68] E. Burstein, N. Vedenkina, M. Ivkova, Fluorescence and the location of tryptophan residues in protein molecules, Photochem. Photobiol. 18 (1973) 263–279.
[69] Z. Amirghofran, M. Bahmani, A. Azadmehr, K. Javidnia, Anticancer effects of various Iranian native medicinal plants on human tumor cell lines, Neoplasma 53 (2005) 428–433.
[70] B. Hemmateenejad, M. Shamsipur, F. Samari, T. Khayamian, M. Ebrahimi, Z. Rezaei, Combined fluorescence spectroscopy and molecular modeling studies on the interaction between harmalol and human serum albumin, J. Pharm. Biomed. Anal. 67 (2012) 201–208.
[71] R.C. Rocha, K. Araki, H.E. Toma, Linkage isomerism, kinetics and electrochemistry of ruthenium-edta complexes of benzotriazole, Transition Met. Chem. 23 (1997) 13–16.
[72] G.G. Mohamed, Z.H.A. El-Wahab, Mixed ligand complexes of bis (phenylimine) Schiff base ligands incorporating pyridinium moiety: synthesis, characterization and antibacterial activity, Spectrochim. Acta Part A 61 (2005) 1059–1068.
[73] Y.-L. Zhang, W.-J. Ruan, X.-J. Zhao, H.-G. Wang, Z.-A. Zhu, Synthesis and characterization of axial coordination cobalt(III) complexes containing chiral Salen ligands, Polyhedron 22 (2003) 1535–1545.
[74] L. Palatinus, G. Chapuis, Superflip–a computer program for the solution of crystal structures by charge flipping in arbitrary dimensions, J. Appl. Crystallogr. 40 (2007) 786–790.
[75] V. Petříček, M. Dušek, L. Palatinus, Crystallographic computing system JANA2006: general features, Z. Kristallogr. Cryst. Mater. 229 (2014) 345–352.
[76] P. Sathyadevi, P. Krishnamoorthy, R.R. Butorac, A.H. Cowley, N. Dharmaraj, Synthesis of novel heterobimetallic copper (I) hydrazone Schiff base complexes: a comparative study on the effect of heterocyclic hydrazides towards interaction with DNA/protein, free radical scavenging and cytotoxicity, Metallomics 4 (2012) 498–511.
[77] X.M. He, D.C. Carter, Atomic structure and chemistry of human serum albumin, Nature 358 (1992) 209–215.
[78] R.L. Joseph, R. Lakowicz, Principles of Fluorescence Spectroscopy, in, Kluwer Academic/Plenum Publishers, New York, 1999.
[79] G. Zhang, N. Zhao, X. Hu, J. Tian, Interaction of alpinetin with bovine serum albumin: probing of the mechanism and binding site by spectroscopic methods, Spectrochim. Acta Part A 76 (2010) 410–417.
[80] R. Patel, M.U.H. Mir, J.K. Maurya, U.K. Singh, N. Maurya, A.B. Khan, A. Ali, Spectroscopic and molecular modelling analysis of the interaction between ethane-1, 2-diyl bis (N, N-dimethyl-N-hexadecylammoniumacetoxy) dichloride and bovine serum albumin, Luminescence 30 (2015) 1233–1241.
[81] J. Lakowicz, Principles of Fluorescence Spectroscopy, third ed., Plenum Press, N.Y., 2006.
[82] M. Niu, M. Hong, S. Cheng, J. Dou, Effect of structure and composition of nickel (II) complexes with salicylidene Schiff base ligands on their DNA/protein interaction and cytotoxicity, J. Inorg. Biochem. 137 (2014) 101–108.
[83] H.-X. Zhang, S. Gao, X.-X. Yang, Synthesis of an octupolar compound and its biological effects on serum albumin, Mol. Biol. Rep. 36 (2009) 1405–1411.
[84] Y.Z. Zhang, X.X. Chen, J. Dai, X.P. Zhang, Y.X. Liu, Y. Liu, Spectroscopic studies on the interaction of lanthanum (III) 2-oxo-propionic acid salicyloyl hydrazone complex with bovine serum albumin, Luminescence 23 (2008) 150–156.
[85] P.D. Ross, S. Subramanian, Thermodynamics of protein association reactions: forces contributing to stability, Biochemistry 20 (1981) 3096–3102.
[86] Y. Zhang, S. Shi, X. Chen, W. Zhang, K. Huang, M. Peng, Investigation on the interaction between ilaprazole and bovine serum albumin without or with different C-ring flavonoids from the viewpoint of food–drug interference, J. Agric. Food Chem. 59 (2011) 8499–8506.
[87] S. Bano, A. Mohd, A.A.P. Khan, K. Siddiqi, Complexation and mechanism of fluorescence quenching of telmisartan with Y (III) and Nd (III), J. Chem. Eng. Data 55 (2010) 5759–5765.
[88] S.H. Choi, K. Pang, K. Kim, D.G. Churchill, Cu2+ Colorimetric sensing and fluorescence enhancement and Hg2+ fluorescence diminution in "scorpionate"-like tetrathienyl-substituted boron-dipyrrins, Inorg. Chem. 46 (2007) 10564–10577.
[89] Y. Xiang, F. Wu, Study of the interaction between a new Schiff-base complex and bovine serum albumin by fluorescence spectroscopy, Spectrochim. Acta Part A 77 (2010) 430–436.
[90] F. Samari, M. Shamsipur, B. Hemmateenejad, T. Khayamian, S. Gharaghani, Investigation of the interaction between amodiaquine and human serum albumin by fluorescence spectroscopy and molecular modeling, Eur. J. Med. Chem. 54 (2012) 255–263.
[91] N. Shahabadi, M. Maghsudi, S. Rouhani, Study on the interaction of food colourant quinoline yellow with bovine serum albumin by spectroscopic techniques, Food Chem. 135 (2012) 1836–1841.
[92] B. Valeur, M.N. Berberan-Santos, Molecular Fluorescence: Principles and Applications, John Wiley & Sons, 2012.
[93] S. Mukhopadhyay, R.K. Gupta, R.P. Paitandi, N.K. Rana, G. Sharma, B. Koch, L.K. Rana, M.S. Hundal, D.S. Pandey, Synthesis, Structure, DNA/Protein Binding, and Anticancer Activity of Some Half-Sandwich Cyclometalated Rh (III) and Ir (III) Complexes, Organometallics 34 (2015) 4491–4506.
[94] P. Krishnamoorthy, P. Sathyadevi, R.R. Butorac, A.H. Cowley, N.S. Bhuvanesh, N. Dharmaraj, Copper (I) and nickel (II) complexes with 1: 1 vs. 1: 2 coordination of ferrocenyl hydrazone ligands: Do the geometry and composition of complexes affect DNA binding/cleavage, protein binding, antioxidant and cytotoxic activities?, Dalton Trans 41 (2012) 4423–4436.
[95] S.E.H. Etaiw, D.M.A. El-Aziz, E.H.A. El-Zaher, E.A. Ali, Synthesis, spectral, antimicrobial and antitumor assessment of Schiff base derived from 2-aminobenzothiazole and its transition metal complexes, Spectrochim. Acta Part A 79 (2011) 1331–1337.
[96] R. Mladenova, M. Ignatova, N. Manolova, T. Petrova, I. Rashkov, Preparation, characterization and biological activity of Schiff base compounds derived from 8-hydroxyquinoline-2-carboxaldehyde and Jeffamines ED®, Eur. Polym. J. 38 (2002) 989–999.
[97] O. Walsh, M. Meegan, R. Prendergast, T. Al Nakib, Synthesis of 3-acetoxyazetidin-2-ones and 3-hydroxyazetidin-2-ones with antifungal and antibacterial activity, Eur. J. Med. Chem. 31 (1996) 989–1000.
[98] Z.-Y. Yang, R.-D. Yang, F.-S. Li, K.-B. Yu, Crystal structure and antitumor activity of some rare earth metal complexes with Schiff base, Polyhedron 19 (2000) 2599–2604.
[99] X. Zhong, J. Yi, J. Sun, H.L. Wei, W.S. Liu, K.B. Yu, Synthesis and crystal structure of some transition metal complexes with a novel bis-Schiff base ligand and their antitumor activities, Eur. J. Med. Chem. 41 (2006) 1090–1092.